The Cryosphere Discuss., 6, 1839–1869, 2012
www.the-cryosphere-discuss.net/6/1839/2012/
doi:10.5194/tcd-6-1839-2012

The Cryosphere Discussions

Thermal conductivity of anisotropic snow measured by three independent methods

F. Riche and M. Schneebeli

WSL Institute for Snow and Avalanche Research SLF, Davos Dorf, Switzerland

Received: 4 April 2012 – Accepted: 30 April 2012 – Published: 25 May 2012

Correspondence to: M. Schneebeli (schneebeli@slf.ch)

Published by Copernicus Publications on behalf of the European Geosciences Union.

Abstract

The thermal conductivity of snow determines the temperature gradient, and by this the rate of snow metamorphism. It is therefore a key property of snow. However, parameterizations of thermal conductivity measured with the transient needle probe and the steady-state heat-flux plate show a bias. In addition, it is not clear to which degree thermal anisotropy is relevant. Until now, no physically convincing argument for the existence of this bias could be found. In this study, we investigated three independent methods to measure snow thermal conductivity and its anisotropy: a needle probe with a long heating time, a guarded heat flux plate, and direct numerical simulation at the level of the pore and ice structure. The three methods were applied to identical snow samples, apart from the different measurement volumes of each methods. We analyzed the consistency and the difference between these methods. We found a distinct change from horizontal thermal anisotropy in small rounded grains and vertical anisotropy in depth hoar. The anisotropy between vertical and horizontal conductivity ranges between 0.5–2. This anisotropy can cause a difference of up to −25 % to +25 % if the thermal conductivity is calculated only from a horizontally inserted needle probe. Based on these measurements, the direct numerical simulation is the most reliable method as the tensorial components of the thermal conductivity can be calculated, the corresponding microstructure is precisely known and the homogeneity of the sample can be determined.

1 Introduction

Thermal conductivity is an important physical property in snow. It is especially important to understand heat transfer and mass flux in snow. Snow has a significant effect on the heat budget, and is very relevant to the climate system (Cook et al., 2007). Thermal conductivity impacts directly the temperature gradient and is therefore one of two fundamental properties determining the rate of snow metamorphism, the other being the

TCD
6, 1839–1869, 2012

heat flux. It is therefore not surprising that first measurements of thermal conductivity of snow were conducted in the late 19th century (for an overview see Sturm et al., 1997). However, science is still struggling to find a general answer what are the most reliable methods to measure effective thermal conductivity, κ_{eff} in snow, and, in a next step, to find the optimal parametrization between microstructure and measurements (Calonne et al., 2011). Recent interest in these questions has increased because inconsistencies between measurements, simulation models and parametrization became apparent (e.g., between Sturm et al., 1997; Calonne et al., 2011).

The reason why the measurement of thermal conductivity in snow is difficult is multifaceted. First, methods are not standardized, and there have been no simultaneous measurements with different instruments on the same snow samples. This is a serious shortcoming, as it is very difficult (impossible) to find the exactly same snow structure twice. The often limited number of measurements makes then the non-linear parameterizations difficult to compare. Second, snow is in many cases extremely fragile, causing artifacts during extraction of the sample or during measurement. As usually only one or very few measurements are made on the same snow type, the inter-sample variability is poorly determined. Third, the microstructural characterization of snow was for a long time semi-quantitative. The recent advent of micro-tomography and stereological techniques allows for a much more precise quantification beyond the porosity, by determining e.g. specific surface area and thickness distributions of ice and air.

Thermal conductivity is important in many different domains, such as food science (Nesvadba, 1982; Cogne, 2003), soil science (Vonherzen and Maxwell, 1959; Abu-Hamdeh and Reeder, 2000) and earth science (Brigaud and Vasseur, 1989; Popov et al., 1999). In all these areas similar problems as in snow are apparent; especially important is the contact problem.

Measurement techniques of thermal conductivity fall in three main classes: steady-state methods, transient methods, and direct numerical simulations. The direct steady-state method uses the heat flux plate.The heat flux plate measures the heat flux through two plates placed at each side of the measured sample. The method is

TCD
6, 1839–1869, 2012

standardized in ASTM (2008). This method was used e.g. by Izumi and Huzioka (1975) and Yamada et al. (1974). Needle probe instruments are based on the transient line heat source method (De Vries, 1952; Blackwell, 1954). They are widely used in snow science (Lange, 1985; Sturm and Johnson, 1992; Morin et al., 2010). A variant, but applied on smooth surfaces, is the divided bar method used to measure the thermal conductivity of rocks and sediments (Pribnow et al., 2000). The Fourier-method, as it was first used by Abels (1892) and recently by Brandt and Warren (1997), measures the approximately sinusoidal temperature change in the ground, and gives a thermal conductivity averaged over the depth of the temperature sensor. In the past about 10 yr, the direct numerical simulation of the thermal conductivity was developed (Ams et al., 2001; Kaempfer et al., 2005; Petrasch et al., 2008; Calonne et al., 2011). This method has the advantage that the 3-D-microstructure together with the well known thermal conductivity of ice and air is sufficient to calculate the effective thermal conductivity of the snow with all components.

A problem, which has received relatively little attention is the thermal anisotropy in snow. Izumi and Huzioka (1975) made a detailed study on the anisotropy of the snow thermal conductivity, and its evolution during temperature gradient metamorphism. The determination of anisotropy will be an important part of this study.

Here we focus on three ways to measure the thermal conductivity of snow: guarded heat flux plate (HFP), single needle probe (NP) and direct numerical simulation (SIM). The main objective is to understand the accuracy and the limitations of these three instruments, under consideration of thermal anisotropy. To compare the methods, we used for all methods the same snow samples, although each method has a differing measurement volume. We analyzed the effect of thermal anisotropy of snow on needle probe measurements and the effect of latent heat flux in HFP measurements. We corrected the measured effective thermal conductivity of the needle probe $\kappa_{\mathrm{eff}}^{\mathrm{NP}}$ for anisotropy. To exclude effects specific to snow, we compared HFP and NP with inert materials over the range of thermal conductivity typical for snow.

TCD
6, 1839–1869, 2012

We do not consider the effect of convection processes on heat transport. Convective processes depend not only on the conductive properties of the material, but also on its permeability (Sturm and Johnson, 1991; Arakawa et al., 2009; Zermatten et al., 2011).

2 Theory

The thermal conductivity in porous media is often not isotropic, but anisotropic. In this case, the effective thermal conductivity κ_{eff} is a tensor (Incropera et al., 2006) (for simplicity of notation, we will write in the following κ for κ_{eff}). If the thermal conductivity is written in tensorial form, then

$$k = -j/\nabla T \tag{1}$$

where k is the thermal conductivity tensor with the components k_x, k_y, k_z, j is the heat flux tensor, and ∇T is the temperature gradient in x, y, z in a Cartesian coordinate system. In the following, we set $k_x = k_y$, because the snowpack has in most cases a horizontal layering. Arons and Colbeck (1995) refers to Izumi and Huzioka (1975) for measurements of anisotropy. However, there are in fact very few measurements measuring tensorial components. Riche and Schneebeli (2010b), measured two components (horizontal k_x and vertical k_z), assuming $k_x = k_y$. Calonne et al. (2011) simulated all tensorial components.

Equation (1) is simplified in all parameterizations (for an overview see Armstrong and Brun, 2008) to one-dimensional form, and $k = k_z$, with k_z the vertical component. If heat flow is measured parallel to the bedding of the snowpack, and the isotherm at the top and the bottom are parallel, then heat flow will be perpendicular to the bedding, independent of an anisotropic structure. Therefore, anisotropy is irrelevant if parameterizations are used under such conditions. However, as we show in this paper, this bias was not always corrected for all instruments, especially in the case of the needle probe. The theory for this case will be introduced in Sect. 2.1.

TCD
6, 1839–1869, 2012

Heat flux in snow is not purely conductive, but as soon as a temperature gradient exists, it has also a latent heat component. Latent heat is generated through the phase change induced by recrystallization (Pinzer and Schneebeli, 2009b). The ratio between conductive heat flux and latent heat flux depends on the absolute temperature and the temperature gradient. We treat this problem in Sect. 2.2.

2.1 Anisotropy

Grubbe et al. (1983) analyzes the case of line source measurements in anisotropic rock. He develops the general case, where the bedding plane is inclined to the surface of the earth. Assuming that NP-measurements in snow are always parallel or orthogonal to the layering of the snowpack, the following formulas can be used. If the z-axis of the coordinate system is orthogonal to the snow surface, then $k_x = k_y$ in the horizontal plane and k_z in the vertical plane. If the needle is horizontally inserted, the following components are measured:

$$k_{\mathrm{h}}^{\mathrm{NP}} = \sqrt{k_x k_z}, \tag{2}$$

with a vertically inserted needle:

$$k_{\mathrm{v}}^{\mathrm{NP}} = \sqrt{k_x^2} \quad \text{for } k_x = k_y. \tag{3}$$

The vertical component k_z can then be extracted from:

$$k_z = \frac{k_{\mathrm{h}}^{\mathrm{NP}2}}{k_x} = \frac{k_{\mathrm{h}}^{\mathrm{NP}2}}{k_{\mathrm{v}}^{\mathrm{NP}}}. \tag{4}$$

We define the anisotropy factor α as $\alpha = k_z/k_x$, which is the inverse of the factor A by Grubbe et al. (1983). α can be better compared qualitatively by the anisotropy

TCD
6, 1839–1869, 2012

factor γ of Izumi and Huzioka (1975), which is defined as $\gamma = (k_z - k_x)/(k_z + k_x)$. The correction for k_z, if the measurement is done with a horizontal needle probe, is then

$$k_z = \sqrt{\alpha} k_{\mathrm{h}}^{\mathrm{NP}}. \tag{5}$$

2.2 Latent heat flux

Pinzer and Schneebeli (2009b) and Pinzer (2009) made direct measurements of the recrystallization rate of snow, and by this the effective latent heat flux. They could show that the vapor diffusivity in snow D_{eff} is close to the diffusivity in air (Giddings and LaChapelle, 1962; Sokratov and Maeno, 2000).

The latent heat flux is calculated using the effective vapor flux present in the snow sample during a heat flux plate experiment. The vapor flux is defined as

$$J_z = D_{\mathrm{H_2O}} \Delta C_z M_{\mathrm{H_2O}}, \quad \text{with} \quad \Delta C_z = \frac{|e_{\mathrm{b}} - e_{\mathrm{t}}|}{h k_{\mathrm{v}} T_{\mathrm{m}}}, \tag{6}$$

where J_z is the heat flux in the z-direction, $D_{\mathrm{H_2O}}$ the water diffusivity, ΔC the gradient of vapor pressure, $M_{\mathrm{H_2O}}$ the mass of a water molecule, e_{b} and e_{t} the pressure according to Murphy and Koop (2005), respectively at top and bottom of the snow sample, h the height of the sample, κ_{B} the Boltzmann constant and T_{m} the mean temperature of the sample.

The latent heat flux is then defined as

$$q_L = J_z L \text{ and } q_t = q_{\mathrm{f}} + q_L, \tag{7}$$

where q_L is the latent heat flux, L the latent heat of sublimation of ice. q_t is the measured heat flow, which includes both the sensible (q_{f}) and the latent (q_L) heat fluxes.

The values used for these equations and the calculation of the latent heat flux are in Appendix A.

TCD
6, 1839–1869, 2012

3 Methods

3.1 Sample preparation

3.1.1 Snow samples

Natural snow blocks were carefully taken from outside. The homogeneity was examined with a SnowMicroPen (Pielmeier, 2003). Each block was used first for the needle probe measurements. Then the block was cut to size for the heat flux plate measurement. In the same block, after the heat flux measurements, two additional horizontal NP-measurements were done. This way, an eventual change due to the HFP-heating could be checked. Finally, the center of the block used for the heat flux plate measurement was carefully inserted in a sample holder for the μ-CT analyses. The inner diameter of the μ-CT sample holder was 36.9 mm. 8 different snow types were analyzed. The snow properties of the samples are shown in Table 1.

Additional snow samples from diverse experiments were used for the direct numerical simulations to calculate the anisotropy of the thermal conductivity. The properties of these samples are shown in Table 2.

3.1.2 Inert samples for calibration

The needle probe and the heat flux plate were calibrated with several common porous and non-porous materials. The range of snow thermal conductivities is 0 and 0.8 $\mathrm{W\,m^{-1}\,K^{-1}}$. We selected materials that cover this range, and in addition can be used both for the HFP and NP. We selected polystyrene foam, plasticine (Fimo), paraffin wax (Glorex), water with 5 % agar-agar (Morga AG). These are similar materials as used by Pinzer and Schneebeli (2009a). In addition, we used granular and sintered coarse-grained sea salt (grain size 2 mm ± 1 mm) as substitute for snow. The absolute thermal conductivity (within better than 10 %) of these non-standard materials is not well known.

TCD
6, 1839–1869, 2012

However, this study was focused on easy and consistent use, which required materials that do not freeze and give minimal contact resistance for both the HFP and NP.

3.2 Measurement of thermal conductivity

3.2.1 Transient measurement with the needle probe

The theory for transient measurements with a needle probe for an ideally conducting material is well known (Blackwell, 1954; Carslaw and Jaeger, 1959; Hartley and Black, 1976). The method is applied forthermal conductivity measurements in snow by different groups (Sturm and Johnson, 1992; Morin et al., 2010).

The thermal conductivity, k^{NP} ($\mathrm{W\,m^{-1}\,K^{-1}}$), was calculated as

$$k = \frac{q}{4\pi\,\Delta T} \ln \frac{t_2}{t_1}, \tag{8}$$

with t_2 (s) and t_1 (s) the linear time region of the measurement, q ($\mathrm{W\,m^{-1}}$) the heating power, ΔT (K) the difference of temperature. Note that the k^{NP} corresponds to k_z only in the case of an isotropic medium.

In this study, we used a needle probe (TP02, Hukseflux Thermal Sensors) with a heating time of 200 s. The needle is 1.2 mm in diameter and 150 mm long. The heating power was $0.07\,\mathrm{W\,m^{-1}}$ in order to have a total temperature increase smaller than −2.5 °C in the snow, which corresponds to a maximal temperature increase of 1 °C in the time interval used in Eq. (8).

To avoid the effect of a high contact resistance, the first 30 s of the measurement were discarded. Convection effects occurred after 100 s. For these reasons, the thermal conductivity was calculated between 30 s to 100 s ($t_1 = 30$ s and $t_2 = 100$ s), which was the linear portion of the measurement curve.

Before use, the accuracy of the needle probe was controlled with measurements in glycerin 80 % (Glycerin CAS 56-81-5).

TCD
6, 1839–1869, 2012

In a homogenous block of snow ($45 \times 45 \times 45\,\mathrm{cm}^3$), with the sides parallel and orthogonal to the layers, two horizontal and two vertical measurements were done. The needle was positioned such that the temperature sensor of the needle was positioned always at the same height of the block. From these four measurements, k_z, k_x and α were calculated.

3.2.2 Steady-state measurement with the guarded heat-flux plate

The guarded heat plate applies a constant heat flux at the bottom of the snow sample, after equilibrium, the heat fluxes at the top and at the bottom of the sample are equal. The difference between the temperatures at both sides of the sample are measured at the same time. As the geometrical properties of the sample are known, the thermal conductivity k^{HFP} ($\mathrm{W\,m^{-1}\,K^{-1}}$)

$$k^{\mathrm{HFP}} = q_{\mathrm{f}} h \frac{1}{\Delta T}, \tag{9}$$

where q_{f} ($\mathrm{W\,m^2}$) is the heat flux across the sample, h (m) the height of the sample and ΔT (K) the temperature difference. If the layering of the sample is parallel to the plates of the apparatus, then $k_z = k^{\mathrm{HFP}}$. In our measurements, the layering was always parallel to the plates.

To avoid convection and snow metamorphism, the applied heat flux and the resulting temperature gradient were kept at ($\nabla T = [10\text{–}15\,\mathrm{K\,m^{-1}}]$) and the temperature at −16 °C.

The design of the HFP is based on the work of Köchle (2009) and is summarized here. The design of the HFP is based on the following points: (i) the heat flux is constant, (ii) the sample is insulated and guarded such that the heat flow is perpendicular to the plates, (iii) the heat flux sensors are guarded by additional surrounding material of equal conductivity, (iv) the temperature difference is measured as precisely as possible, (v) the size of the sample chamber must be sufficiently large that an undisturbed snow sample can be used. We built an apparatus with a plate size of 210 × 210 mm and

TCD
6, 1839–1869, 2012

adjustable height between 5 and 80 mm. The base of the chamber consisted of 30 mm styrofoam insulation. On top of the insulation, a film heater (Minco, Type HK5170) was glued to a steel plate (8 mm thick), which served to distribute heat and damped any remaining fluctuations by the inherent heat capacity. A polycarbonate plate (3 mm thick) with a center hole of 100 mm followed. The center hole was filled with the heat flux sensor (Hukseflux PU_43), with a diameter of 100 mm and 3 mm thick, and an active sensing area of 30 × 30 mm. The total error of the heat flux measurement was ±0.1 $W m^{-2}$ at the typical heat flux of 2 $W m^{-2}$. The outer area served as a thermal shield for the sensor. Polycarbonate plate and heat flux sensor have the same thermal conductivity of 0.25 $W m^{-1} K^{-1}$. Then the snow sample, usually 60 mm thick, followed. The sample was covered again with a heat flux sensor and polycarbonate plate, and a 6 mm thick aluminum plate improved contact further. The polycarbonate plates where covered with a thin layer of thermal grease (Dow Corning 340, $k = 0.55 W m^{-1} K^{-1}$) to reduce the contact resistance between snow and plate. The temperature difference between the plates was measured using two K-type thermocouples in series, such that directly the temperature difference was measured across the snow. The precision of the thermocouple in series was ±0.03 K. The absolute temperature was measured at the bottom of the plate using a RTD-sensor (Minco, Type S17621) with an absolute precision of ±0.4 °C. The sides of the apparatus were covered with 30 mm styrofoam insulation. The HFP-apparatus was housed in an insulated chamber (dimension 70 × 70 × 80 cm), which was heated up to −15 °C in a cold laboratory kept −20 °C, to reduce temperature variations, which affected the stability of the measurements. All data logging was done with a Campbell CR10 data logger.

3.3 Tomography and direct numerical simulation

Each sample was directly measured, without further preparation, in the μ-CT (Scanco micro-CT80). The temperature during measurement was controlled and kept constant at −15 °C. The nominal resolution of the images was 18 µm. The size of the original

TCD
6, 1839–1869, 2012

image was 2048 × 2048 × 416 voxels, the scanned volume had a diameter of 36 mm and was 7.5 mm high.

3.3.1 Image processing

From the μ-CT measurements, a volume of 400 × 400 × 400 voxels (7.2 mm × 7.2 mm × 7.2 mm) was extracted from the original data. This volume was then segmented to a binary image. A Gauss filter ($\sigma = 1$, support = 2) was applied and the ice structure segmented using an adaptive threshold. The obtained density of the ice volume was compared to the measured density of the snow sample as control for the segmentation. If the difference in density was higher than 12 %, the threshold in the segmentation process was manually corrected to obtain the right density within 12 %. Depth hoar samples were rescaled to a nominal resolution of 36 µm. This was necessary to conduct the direct numerical simulation within a reasonable time and with a larger representative elementary volume (REV) of a sufficient size (volume of $10.8 \times 10.8 \times 10.8\,\mathrm{mm}^3$). From each sample, except depth hoar, two subsamples where taken to receive an estimate of intra-sample variability.

3.3.2 Direct numerical simulation

The numerical simulation is based on Kaempfer and Plapp (2009) and Pinzer (2009). The simulation required the temperature gradient in the snow and the thermal conductivity of air and ice. We used the following values: $\nabla T = 50\,\mathrm{K\,m^{-1}}$, $k_{\mathrm{ice}} = 2.34\,\mathrm{W\,m^{-1}\,K^{-1}}$ (k_{ice} at −20 °C, Slack, 1980) and $k_{\mathrm{air}} = 0.024\,\mathrm{W\,m^{-1}\,K^{-1}}$. Based on the simulated heat flux and the prescribed temperature gradient the thermal conductivity was calculated:

$$k_{x,z}^{\mathrm{SIM}} = q_{x,z}/\nabla T. \tag{10}$$

For each k_z and k_x an independent simulation was necessary.

TCD
6, 1839–1869, 2012

4 Results

4.1 Calibration of the needle probe and the heat flux plate

We measured the thermal conductivity of the inert materials (polystyrene foam, plasticine, wax at room temperature and at cold lab temperature (−20 °C), agar gel (5 %), and salt in granular form and as a sintered block) with the needle probe and the heat flux plate (Fig. 2). In homogenous, isotropic and non porous materials (plasticine, polystyrene, wax), k^{NP} and k^{HFP} were similar. k^{NP} was slightly higher than k^{HFP} for agar, but k^{NP} was 30–40 % lower than k^{HFP} for the granular salt. Similarly, a long heating time resulted in a 15 % lower k^{NP} than k^{HFP} for the sintered salt block. A short heating resulted in a k^{NP} 70 % lower than the two other measurements.

A linear regression was calculated for the short and the long heating time NP versus HFP, forcing the curve through the origin. The measurement of the salt block at short heating time was removed from the regression. The correlation between NP measurements and HFP measurements was high ($R = 0.946$). We found that the regression equation for both the short and long heating time was $k^{NP} = 0.96k^{HFP}$ with a root mean square error (deviation) of 0.07, and all points within 99 % significance.

4.2 Numerical simulation

The thermal conductivity was calculated for all samples of Table 1 (all measured and calculated thermal conductivities are in the Supplement). Each sample was calculated for two independent volumes, except for the depth hoar sample. The size of the REV was too large to extract two independent volumes from the scanned volume. Density and thermal conductivity of these samples are shown in Fig. 6 (and in supplementary material Table 1). The density of the two paired samples varied between 0.1–3.2 %, (average 1.3 %), the thermal conductivity between 0.5–34 % (average 6.1 %). The outlier with 34 % was for the faceted snow with a density of 261 kg m^{-3} .

TCD
6, 1839–1869, 2012

The simulation depended on the selection of the threshold for the segmentation of the ice structure. To test for the sensitivity, we increased the threshold by 10 % for one sample. This increased the volumetric density by 4 % and the thermal conductivity by 8 %. However, a change of the threshold by 10 % is obvious when comparing the gray-scale images with the segmented image, and is therefore a worst-case assumption.

4.3 Comparison of the needle probe and simulation

The vertical and horizontal thermal conductivity of long heating-time NP, corrected for anisotropy, were systematically lower by 10–35 % compared to the direct numerical simulation (Fig. 3). We found that the trend in anisotropy is in most cases the same ($k_x^{SIM} > k_z^{SIM}$ if $k_x^{NP} > k_z^{NP}$). The correlation between k^{SIM} and k^{NP} was $k^{NP} = 0.79k^{SIM} - 0.021$ ($r^2 = 0.75$, residual mean square error 0.023). The difference between the null hypothesis (the 1 : 1 curve) and the correlation was significant at the 99 %-level.

4.4 Intercomparison of all methods

The vertical components of k_z for NP were in all samples lower than HFP and SIM (Fig. 4). k_z^{SIM} are 3 % to 25 % lower (average 20 %) than k_z^{HFP} and k_z^{NP} are 15 % to 55 % lower (average 35 %) than HFP (Fig. 5). The differences between NP compared to SIM and HPA were highly significant, and the difference between SIM and HPA was significant.

The comparison of the relative change of k_h^{NP} between the two NP-measurements before and after the HFP-measurements showed a mean increase of 6.3 % ± 8.4 % (minimum −4.9 %, maximum +18.5 %).

4.5 Anisotropy factor

$k_{z,y}^{SIM}$ was calculated for 35 samples in total. The temperature for ice and air was always set to −20 °C (Fig. 6). We found that the majority of samples were to a certain degree

TCD
6, 1839–1869, 2012

anisotropic, and isotropic snow seemed to be rather the exception than the rule. The anisotropy factor γ (Izumi and Huzioka, 1975) was calculated for comparison. For the 35 samples, γ was between −0.23 to 0.31. The anisotropy of our snow samples with a similar snow structure and density showed the same pattern as those of Izumi and Huzioka (1975).

4.6 Latent heat flux in the HFP

All measured values in the HFP were measured at a temperature of $-16\,^{\circ}\mathrm{C} \pm 1\,^{\circ}\mathrm{C}$, to reduce latent heat flux. For a temperature gradient of $11\,\mathrm{K\,m^{-1}}$, the calculated latent heat flux was $0.01\,\mathrm{W\,m^{-2}}$. In the HFP measurement, the heat flux was approximately $2\,\mathrm{W\,m^{-2}}$, therefore the latent heat flux represented less than 1 % of the measured heat flux. The latent heat flux had therefore no significant effect on the heat flux at this temperature. However, at higher temperatures, latent heat flux becomes significant, at a temperature of $-5\,^{\circ}\mathrm{C}$ and the same temperature gradient; the latent heat flux would increase to $0.14\,\mathrm{W\,m^{-2}}$, corresponding to a contribution of 14 %.

5 Discussion

The thermal conductivities of NP and HFP in the inert, isotropic and solid reference materials lie almost perfectly on a 1 : 1 curve. Both methods, NP and HFP, gave the same absolute values of thermal conductivity in these materials. Both instruments showed no temperature dependence, tested with wax at 20 °C and −20 °C. The higher k^{NP} with agar was caused by convection, and was also observed by Boumaza and Redgrove (2003). The NP measurement in sintered salt with short heating time (30 s) is a reminder that NPs with short heating time do not measure correctly the thermal conductivity due to contact resistance problems in porous materials (Riche and Schneebeli, 2010a). The long-heating time NP-measurements in granular and sintered salt resulted in significantly lower values (50 % for granular salt grains, 20 % for sintered salt grains)

TCD
6, 1839–1869, 2012

than the HFP-measurements. We think that there are two possible reasons. The first is that the poor contact resistance influenced the linearity within the evaluated timespan. However, a longer measurement time was not possible (longer than 100 s), because of the clearly visible onset of convective processes (Sturm and Johnson, 1992). The second reason could be be the heterogeneity of the temperature field. It is well known for the measurement of dielectric properties that the radius of curvature of the electrode must be much larger than the snow grain diameter (Mätzler, 1996). The size of the salt-grains was about twice the size of the diameter of the needle probe, so the empirical rule would be clearly violated.

The difference between HFP and SIM could be caused by two factors. The thermal grease applied could increase the thermal conductivity and therefore a correction in the effective height would be necessary. A 2 mm thick layer of thermal grease on both plates would lead to an increase of about 5 % in k^{SIM}. Such a correction was not applied. Another reason could be that the finite resolution of the μ-CT and the thresholding eliminated heat-conducting bonds. These two factors lead to a maximal absolute uncertainty of k by 10–15 %. This result is comparable to Calonne et al. (2011).

k^{NP} compared k^{SIM} gave consistent results, in the sense that the relative difference was constant (Fig. 3). However, k^{NP} corrected for anisotropy were again significantly lower than k^{SIM} and k^{HFP}. Riche and Schneebeli (2010a) show that the microstructural changes around the needle can be visible and large, but suggested that this effect was only important for short heating times. Measurements in glycerin show no effect of an air gap on the thermal conductivity (M. Sturm and J. B. Johnson, personal communication). Calonne et al. (2011) suggests the measured volume around the needle probe is too small. As for the salt grains, another explanation could be that the thermal field is too far from homogenous conditions for such a thin needle probe to apply the theory developed for transient methods (Blackwell, 1954; Mätzler, 1996).

By comparison, HFP always gave values higher than the SIM and NP (Fig. 4). The difference between HFP and SIM can mainly be explained by its sensitivity relative to the snow density. It happened that the densities of the μ-CT-measurements were lower

TCD
6, 1839–1869, 2012

than the measured density of the snow. This effect will cause simulated values lower than the real thermal conductivity value. HFP-methods are considered as less reliable than NP, because they are more susceptible to measurement induced metamorphism (Sturm and Johnson, 1992). We observed such a predicted increase of k on the order of 5 % (see Sect. 4.4). However, this increase did not explain the much larger difference between NP compared to SIM and HFP.

Izumi and Huzioka (1975) and Yamada et al. (1974) showed the existence of anisotropic thermal conductivity in snow. We found that anisotropy is considerable for most snow types. The only new snow sample was isotropic, small rounded grains had an $\alpha < 1$, and faceted snow and depth hoar had in general $\alpha < 1$. All depth hoars with a density above 200 kg m^{-3} had an α between 1.25–1.75. Melt forms covered a very broad range of α between 0.75–1.75, probably depending on the anisotropy before wet snow metamorphism started. Our measurements corroborate that k_h^{NP} must be corrected by Eq. (5) to give a correct k_z. This correction as proposed by Grubbe et al. (1983) clearly reduced the difference between NP and SIM. The most comprehensive datasets of thermal conductivity (Sturm et al., 2002, 1997; Sturm and Johnson, 1992) and their parametrization should be corrected for anisotropy depending on grain type and density. Such a correction is also necessary in homogenous layers, and should be done in future measurements, especially for long-term measurements with needle-probes (Morin et al., 2010). However, NP shows still a systematic bias to SIM and NP, even after correction for anisotropy.

Snow pack models are currently one-dimensional (Etchevers et al., 2004), and therefore k_z is most relevant. If the measured anisotropy is not parallel to the surface in certain landscapes (hummocky tundra, boulder covered areas, sea ice) needs further investigation. This could have important ramifications for heat flow and energy balance in complex terrain.

Based on the results of Sokratov and Maeno (2000) and Pinzer (2009) the latent heat flux could be estimated within a factor of two. The latent heat flux was considered before as a major weak point in the use of HFP. The calculated latent heat fluxes at the

TCD
6, 1839–1869, 2012

low temperatures used were less than 1 % in the worst case, and therefore negligible. The higher thermal conductivity of the HFP measurements compared to SIM could not be explained by this reason. To some degree, the thermal grease applied between the plates could cause about 5 % increase, but does not explain the complete difference.

6 Conclusions

We used identical snow for three different methods to measure the thermal conductivity of snow. This allowed to limit the reasons for systematic differences found between methods. HFP gave consistently to high results compared with the direct numerical simulation, and the the NP systematically underestimated the thermal conductivity of snow, even after correction for anisotropy. We showed that NP measures a lower κ_{eff} in dry sintered salt. In addition, κ_{eff} remains after correction for anisotropy lower than κ_{eff} measured with HFP.

We found that many snow types are anisotropic regarding thermal conductivity. This makes measurements using the NP difficult, as at least one horizontal and one vertical measurement is required, and the individual layers must be sufficiently (at least a few cm) thick. Natural anisotropy can cause an error of ± 25 %. We also found that anisotropy is weakly correlated with grain shape. However, the scatter is very large, and a correction for anisotropy will be difficult.

We found that the reproducibility of all methods was similar, with relative differences between the methods of about ± 10 %. The HFP proved to be reliable. The necessary temperature gradient increased however the thermal conductivity by about 6 % on average. HFP are very time-consuming, and best suited for laboratory experiments. In combination with direct numerical simulations, they could also be used to investigate the effect of latent heat flux on the microstructure.

The current design of the needle probe has therefore two problems, the first is a systematically too low value, and the second that at least two measurements are necessary to determine the anisotropy of the thermal conductivity. HFP and SIM gave similar

TCD
6, 1839–1869, 2012

results. However, HFP is a very time-consuming method and measure only k_z. Direct numerical simulations is possibly the most precise way to to obtain reliable values of the effective thermal conductivity of snow. Recent improvements in imaging the microstructure of snow make this method widely available.

Appendix A

Calculation of the latent heat flux

The relevant constants for the calculation of the latent heat flux in snow are: Avogadro number: $N_a = 6.022 \cdot 10^{23}$ (particles per mole), mass of a water molecule: $M_{H_2O} = 18.016 \cdot 10^{-3}/N_a$ (kg), Boltzmann constant: $k_B = 1.38065 \cdot 10^{-23}$ (JK^{-1}), water diffusivity: $D_{H_2O} = 2.178 \cdot 10^{-5} \cdot (1013/840.0) \cdot ((T_{mean} + 273.15)/273.15)^{1.81}$ ($m^2 s^{-1}$), latent heat of ice: $3.34 \cdot 10^5$ (Jkg^{-1}).

The vapor flux in our experiments was calculated as follows: the mean temperature was $T_{mean} = 257\,K$, the bottom temperature was $T_{bot} = 257.25\,K$, the top temperature was $T_{top} = 256.75\,K$ and the height of the snow sample was $h = 4.5 \cdot 10^{-2}\,m$.

The top and bottom pressure were calculating according to Murphy and Koop (2005):

bottom pressure: $e_b = e^{(9.55 - 5723.265/T_{bot} + 3.53068 \cdot \log(T_{bot}) - 0.00728332 \cdot T_{bot})}$,

top pressure: $e_t = e^{(9.55 - 5723.265/T_{top} + 3.53068 \cdot \log(T_{top}) - 0.00728332 \cdot T_{top})}$.

By applying Eq. (7), we obtained $J_z = 3.088 \cdot 10^{-8}\,kg\,m^{-2}\,s^{-1}$ and from Eq. (6): $q_L = 0.0103\,W\,m^{-2}$.

Supplementary material related to this article is available online at: http://www.the-cryosphere-discuss.net/6/1839/2012/tcd-6-1839-2012-supplement.pdf.

TCD
6, 1839–1869, 2012

Acknowledgements. This work is supported by the Swiss National Science Foundation. The authors thank B. Köchle for the HFP snow measurements, and M. Sturm and J. B. Johnson for the needle probe and discussions, C. Mätzler to bring up the idea of the homogeneity of the temperature field.

References

Abels, G.: Beobachtungen der täglichen Periode der Temperatur im Schnee und Bestimmung des Wärmeleitungsvermögens des Schnees als Function seiner Dichtigkeit, Kaiserl. Akad. Wissensch., Rep. Meteorologie, 16, 1–53, 1892. 1842

Abu-Hamdeh, N. and Reeder, R.: Soil thermal conductivity: effects of density, moisture, salt concentration, and organic matter, Soil Sci. Soc. Am. J., 64, 1285–1290, 2000. 1841

Ams, C. H., Knackstedt, M. A., Pinczewski, W. V., and Lindquist, W. B.: Accurate estimation of transport properties form microtomographic images, Geophys. Res. Lett., 28, 3361–3364, 2001. 1842

Arakawa, H., Izumi, K., Kawashima, K., and Kawamura, T.: Study on quantitative classification of seasonal snow using specific surface area and intrinsic permeability, Cold Reg. Sci. Technol., 59, 163–168, doi:10.1016/j.coldregions.2009.07.004, 2009. 1843

Armstrong, R. L. and Brun, E.: Snow and Climate, Physical Porcesses, Surface Energy Exchange and Modeling, Chapt. 4.4, Cambridge University Press, New York, USA, 2008. 1843

Arons, E. M. and Colbeck, S. C.: Geometry of heat and mass transfer in dry snow: a review of theory and experiment, Rev. Geophys., 33, 463–493, doi:10.1029/95RG02073, 1995. 1843

ASTM: Test method for steady-state heat flux measurements and thermal transmission properties by means of the guarded-hot-plate apparatus, in: Annual Book of ASTM Standards, vol. C 177, ASTM International, West Conshohocken, PA, USA, doi:10.1520/C0177-10, 2008. 1842

Blackwell, J. H.: A transient-flow method for determination of thermal constants of insulating materials in bulk. 1. Theory, J. Appl. Phys., 25, 137–144, 1954. 1842, 1847, 1854

Boumaza, T. and Redgrove, J.: Use of the transient plane source technique for rapid multiple thermal property measurements, Int. J. Thermophys., 24, 501–512, 2003. 1853, 1865

Brandt, R. E. and Warren, S. G.: Temperature measurements and heat transfer in near-surface snow at the South Pole, J. Glaciol., 43, 339–351, 1997. 1842

TCD

6, 1839–1869, 2012

Brigaud, F. and Vasseur, G.: Mineralogy, porosity and fluid control on thermal-conductivity of sedimentary-rocks, Geophys. J. Int., 98, 525–542, 1989. 1841
Calonne, N., Flin, F., Morin, S., Lesaffre, B., du Roscoat, S. R., and Geindreau, C.: Numerical and experimental investigations of the effective thermal conductivity of snow, Geophys. Res. Lett., 38, L23501, doi:10.1029/2011GL049234, 2011. 1841, 1842, 1843, 1854
Carslaw, H. S. and Jaeger, J. C.: Conduction of Heat in Solids, 2 Edn., Clarendon Press, New York, USA, 1959. 1847
Cogne, C.: Experimental data and modelling of thermal properties of ice creams, J. Food Eng., 58, 331–341, doi:10.1016/S0260-8774(02)00396-5, 2003. 1841
Cook, B. I., Bonan, G. B., Levis, S., and Epstein, H. E.: The thermoinsulation effect of snow cover within a climate model, Clim. Dynam., 31, 107–124, doi:10.1007/s00382-007-0341-y, 2007. 1840
De Vries, D.: A nonstationary method for determining thermal conductivity of soil in situ, Soil Sci., 73, 83–89, 1952. 1842
Etchevers, P., Martin, E., Brown, R., Fierz, C., Lejeune, Y., Bazile, E., Boone, A., Dai, Y.-J., Essery, R., Fernandez, A., Gusev, Y., Jordan, R., Koren, V., Kowalczyk, E., Nasonova, N. O., Pyles, R. D., Schlosser, A., Shmakin, A. B., Smirnova, T. G., Strasser, U., Verseghy, D., Yamazaki, T., and Yang, Z.-L.: Validation of the energy budget of an alpine snowpack simulated by several snow models (SnowMIP project), Ann. Glaciol., 38, 150–158, doi:10.3189/172756404781814825, 2004. 1855
Giddings, J. C. and LaChapelle, E.: The formation rate of depth hoar, J. Geophys. Res., 67, 2377–2383, doi:10.1029/JZ067i006p02377, 1962. 1845
Grubbe, K., Haenel, R., and Zoth, G.: Determination of the vertical component of thermal conductivity by line source methods, Zbl. Geo. Pal. 1, 49–56, 1983. 1844, 1855, 1864
Hartley, J. G. and Black, W. Z.: Minimization of measurement errors involved in probe method of determining soil thermal-conductivity, J. Heat Trans.-T. ASME, 98, 530–531, 1976. 1847
Incropera, F. P., Dewitt, D. P., Bergman, T. L., and Lavine, A. S.: Fundamentals of Heat and Mass Transfer, 6th edn., Wiley, USA, 2006. 1843
Izumi, K. and Huzioka, T.: Studies of metamorphism and thermal conductivity of snow, I, Low Temp. Sci. A, 33, 91–102, 1975. 1842, 1843, 1845, 1853, 1855
Kaempfer, T. and Plapp, M.: Phase-field modeling of dry snow metamorphism, Phys. Rev. E, 79, 17, doi:10.1103/PhysRevE.79.031502, 2009. 1850

TCD
6, 1839–1869, 2012

Kaempfer, T. U., Schneebeli, M., and Sokratov, S. A.: A microstructural approach to model heat transfer in snow, Geophys. Res. Lett., 32, L21 503, doi:10.1029/2005gl023873, 2005. 1842
Köchle, B.: Thermal Conductivity of Snow, Ph.D. thesis, Karl-Franzens Universität Graz, 2009. 1848
Lange, M. A.: Measurements of thermal parameters in antarctic snow and firn, Ann. Glaciol., 6, 100–104, 1985. 1842
Mätzler, C.: Microwave permittivity of dry snow, IEEE T. Geosci. Remote, 34, 573–581, doi:10.1109/36.485133, 1996. 1854
Morin, S., Domine, F., Arnaud, L., and Picard, G.: In-situ monitoring of the time evolution of the effective thermal conductivity of snow, Cold Reg. Sci. Technol., 64, 73–80, doi:10.1016/j.coldregions.2010.02.008, 2010. 1842, 1847, 1855
Murphy, D. M. and Koop, T.: Review of the vapour pressures of ice and supercooled water for atmospheric applications, Q. J. Roy. Meteorol. Soc., 131, 1539–1565, doi:10.1256/Qj.04.94, 2005. 1845, 1857
Nesvadba, P.: Methods for the measurement of thermal conductivity and diffusivity of foodstuffs, J. Food Eng., 1, 93–113, 1982. 1841
Petrasch, J., Schrader, B., Wyss, P., and Steinfeld, A.: Tomography-based determination of the effective thermal conductivity of fluid-saturated reticulate porous ceramics, J. Heat Transf., 130, 032602, doi:10.1115/1.2804932, 2008. 1842
Pielmeier, C.: Stratigraphy and changes in hardness of snow measured by hand, ramsonde and snow micro penetrometer: a comparison with planar sections, Cold Reg. Sci. Technol., 37, 393–405, doi:10.1016/S0165-232X(03)00079-X, 2003. 1846
Pinzer, B. R.: Dynamics of Temperature Gradient Snow Metamorphism, Ph.D. thesis, ETH Zurich Nr. 18456, 2009. 1845, 1850, 1855
Pinzer, B. and Schneebeli, M.: Breeding snow: an instrumented sample holder for simultaneous tomographic and thermal studies, Meas. Sci. Technol., 20, 095 705, doi:10.1088/0957-0233/20/9/095705, 2009a. 1846
Pinzer, B. R. and Schneebeli, M.: Snow metamorphism under alternating temperature gradients: morphology and recrystallization in surface snow, Geophys. Res. Lett., 36, L23 503, doi:10.1029/2009GL039618, 2009b. 1844, 1845
Popov, Y. A., Pribnow, D. F. C., Sass, J. H., Williams, C. F., and Burkhardt, H.: Characterization of rock thermal conductivity by high-resolution optical scanning, Geothermics, 28, 253–276, doi:10.1016/S0375-6505(99)00007-3, 1999. 1841

TCD
6, 1839–1869, 2012

Pribnow, D. F. C., Davis, E. E., and Fisher, A. T.: Borehole heat flow along the eastern flank of the Juan de Fuca Ridge, including effects of anisotropy and temperature dependence of sediment thermal conductivity, J. Geophys. Res.-Sol. Ea., 105, 13449–13456, 2000. 1842

Riche, F. and Schneebeli, M.: Microstructural change around a needle probe to measure thermal conductivity of snow, J. Glaciol., 56, 871–876, doi:10.3189/002214310794457164, 2010a. 1853, 1854

Riche, F. and Schneebeli, M.: Anisotropy evolution of thermal conductivity in natural snow evaluated with X-ray tomography and computer simulations, AGU Fall Meeting Abstracts, A511, San Fransisco, 2010b. 1843

Slack, G.: Thermal conductivity of ice, Phys. Rev. B, 22, 3065–3071, 1980. 1850

Sokratov, S. A. and Maeno, N.: Effective water vapor diffusion coefficient of snow under a temperature gradient, Water Resour. Res., 36, 1269–1276, doi:10.1029/2000WR900014, 2000. 1845, 1855

Sturm, M. and Johnson, J. B.: Natural convection in the subarctic snow cover, J. Geophys. Res., 96, 11657–11671, doi:10.1029/91JB00895, 1991. 1843

Sturm, M. and Johnson, J. B.: Thermal conductivity measurements of depth hoar, J. Geophys. Res., 97, 2129–2139, doi:10.1029/91JB02685, 1992. 1842, 1847, 1854, 1855

Sturm, M., Holmgren, J., König, M., and Morris, K.: The thermal conductivity of seasonal snow, J. Glaciol., 43, 26–41, 1997. 1841, 1855

Sturm, M., Perovich, D. K., and Holmgren, J.: Thermal conductivity and heat transfer through the snow on the ice of the Beaufort Sea, J. Geophys. Res.-Oceans, 107, 8043, doi:8043 10.1029/2000jc000409, 2002. 1855

Vonherzen, R. and Maxwell, A. E.: The measurement of thermal conductivity of deep-sea sediments by a needle-probe method, J. Geophys. Res., 64, 1551–1563, 1959. 1841

Yamada, T., Hasemi, T., Izumi, K., and Sato, A.: On the dependencies of the velocities of P- and S-waves and thermal conductivity of snow upon the texture of snow, Low Temp. Sci. A, 32, 71–80, 1974. 1842, 1855

Zermatten, E., Haussener, S., Schneebeli, M., and Steinfeld, A.: Instruments and methods tomography-based determination of permeability and Dupuit–Forchheimer coefficient of characteristic snow samples, J. Glaciol., 57, 811–816, 2011. 1843

TCD
6, 1839–1869, 2012

Table 1. Structural properties of the snow samples[a].

Snow Type	ISC	Density $kg\,m^{-3}$	SSA mm^{-1}	i.th mm	i.sp mm
Depth hoar	DHch	172	12.90	0.20 ± 0.07	1.76 ± 1.27
Facets	FCso	230	12.71	0.25 ± 0.07	0.42 ± 0.15
Small rounded	RGxf	246	17.63	0.17 ± 0.04	0.36 ± 0.14
Small rounded	FCxr	251	17.05	0.18 ± 0.05	0.40 ± 0.14
Small rounded	RGsr	253	14.47	0.22 ± 0.05	0.30 ± 0.13
Large rounded	RGlr	267	16.16	0.19 ± 0.07	0.41 ± 0.16
Small rounded	RGsr	286	8.84	0.34 ± 0.13	0.81 ± 0.36
Small rounded	RGsr	331	19.89	0.16 ± 0.03	0.27 ± 0.09

[a] Snow type: description, ISC: International Classification, Density: gravimetrically determined, SSA: specific surface area from tomography, i.th: thickness of ice structures by tomography, i.sp: pore size by tomography.

TCD
6, 1839–1869, 2012

Table 2. Structural properties of the additionnal snow samples used for the simulation of thermal conductivity anisotropy[a].

Snow Type	ISC	Density $kg\,m^{-3}$	SSA mm^{-1}	i.th mm	i.sp mm
New snow	PPsd	91	64.65	0.05 ± 0.03	0.45 ± 0.19
Small rounded	RGsr	118	25.09	0.13 ± 0.04	0.56 ± 0.34
Small rounded	RGsr	155	29.03	0.12 ± 0.03	0.31 ± 0.11
Small rounded	RGsr	155	27.15	0.12 ± 0.03	0.33 ± 0.12
Small rounded	RGsr	164	26.78	0.12 ± 0.03	0.34 ± 0.13
Small rounded	RGsr	173	23.41	0.14 ± 0.04	0.36 ± 0.14
Small rounded	RGsr	182	25.50	0.13 ± 0.03	0.30 ± 0.11
Small rounded	RGsr	191	26.39	0.13 ± 0.03	0.28 ± 0.10
Small rounded	RGsr	191	24.90	0.13 ± 0.03	0.32 ± 0.12
Small rounded	RGsr	191	31.34	0.10 ± 0.03	0.24 ± 0.09
Small rounded	RGsr	200	24.85	0.13 ± 0.04	0.29 ± 0.11
Depth hoar	DHcp	209	12.28	0.23 ± 0.14	0.93 ± 0.53
Depth hoar	DHcp	228	11.31	0.25 ± 0.13	0.78 ± 0.37
Depth hoar	DHcp	237	15.99	0.17 ± 0.07	0.49 ± 0.23
Depth hoar	DHcp	237	16.37	0.16 ± 0.07	0.47 ± 0.22
Facets	FCso	246	11.65	0.26 ± 0.09	0.54 ± 0.21
Depth hoar	DHcp	246	10.51	0.29 ± 0.20	0.82 ± 0.44
Depth hoar	DHcp	255	12.97	0.20 ± 0.10	0.62 ± 0.33
Melt-refrozen	MFcl	264	8.21	0.35 ± 0.13	0.80 ± 0.35
Large rounded	RGlr	264	11.89	0.26 ± 0.09	0.49 ± 0.20
Melt-refrozen	MFcl	273	9.40	0.31 ± 0.12	0.63 ± 0.29
Depth hoar	DHcp	282	14.05	0.17 ± 0.07	0.54 ± 0.32
Melt-refrozen	MFcl	282	14.72	0.21 ± 0.06	0.34 ± 0.13
Depth hoar	DHcp	291	13.51	0.19 ± 0.10	0.51 ± 0.28
Melt-refrozen	MFcl	300	15.14	0.21 ± 0.06	0.31 ± 0.12
Facets	FCso	309	7.11	0.41 ± 0.18	0.71 ± 0.29
Melt-refrozen	MFcl	364	9.62	0.31 ± 0.11	0.40 ± 0.17

[a] Snow type: description, ISC: International Classification, Density: gravimetrically determined, SSA: specific surface area from tomography, i.th: thickness of ice structures by tomography, i.sp: pore size by tomography.

TCD
6, 1839–1869, 2012

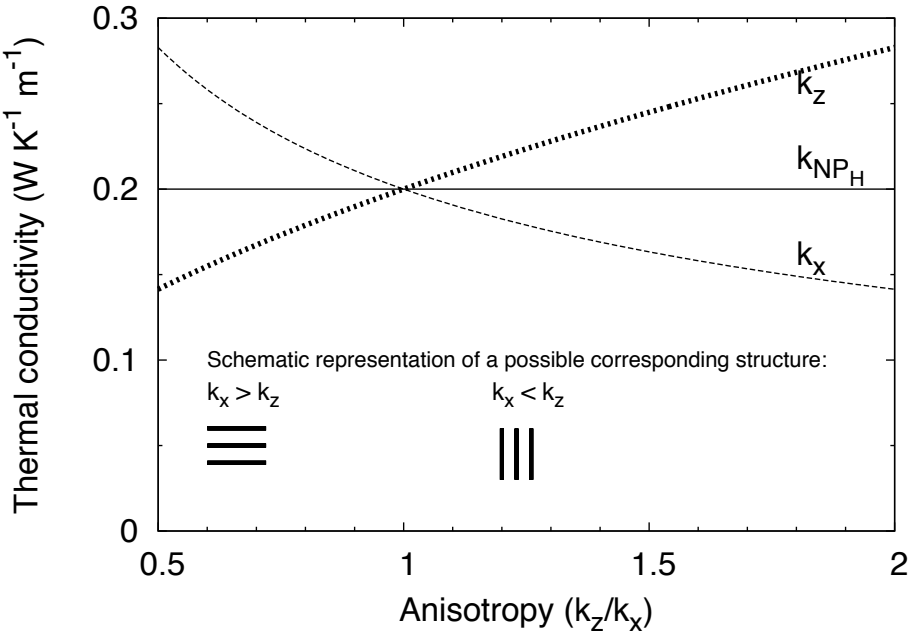

Fig. 1. The effect of anisotropy of snow on the effective vertical thermal conductivity if thermal conductivity is measured with a horizontal needle probe. Calculations are based on Grubbe et al. (1983). The range of the anisotropy factor between 0.5 to 2 is typical for natural snow. The horizontal line at 0.2 $W m^{-1} K-1$ indicates the measured thermal conductivity with the needle probe horizontally inserted. For an anisotropy factor α less than 1 the effective vertical thermal conductivity is underestimated by up to 25 %. In case of an anisotropy factor larger than 1, k_v^{eff} is underestimated by up to 25 %. Also shown is the horizontal component of the thermal conductivity, $k_x = k_v^{NP}$, which corresponds to the value measured with a vertically inserted needle probe.

TCD
6, 1839–1869, 2012

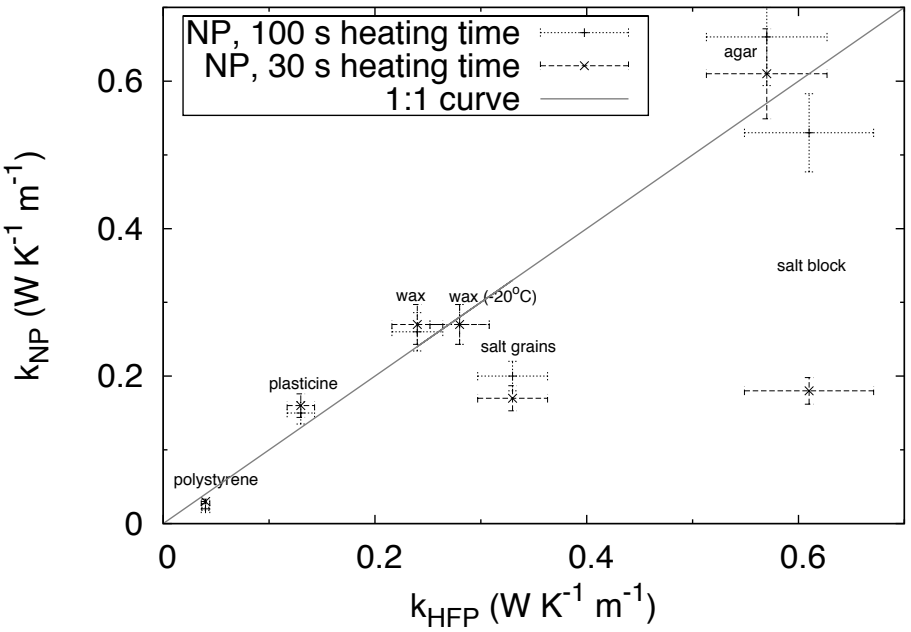

Fig. 2. Intercomparison between heat flux plate (HFP) and needle probe (NP), measured on inert, partially porous, isotropic materials. HFP and NP are on a 1 : 1 line for inert, non-porous materials. Measurements in agar are known to be to high due to convection (Boumaza and Redgrove, 2003). The needle probes measure a two low value compared to the HFP for the porous materials (granular salt grains and sintered sea salt). The k^{NP} resulting from a 100 s instead of 30 s measurement increases thermal conductivity almost threefold for the sintered salt block.

TCD
6, 1839–1869, 2012

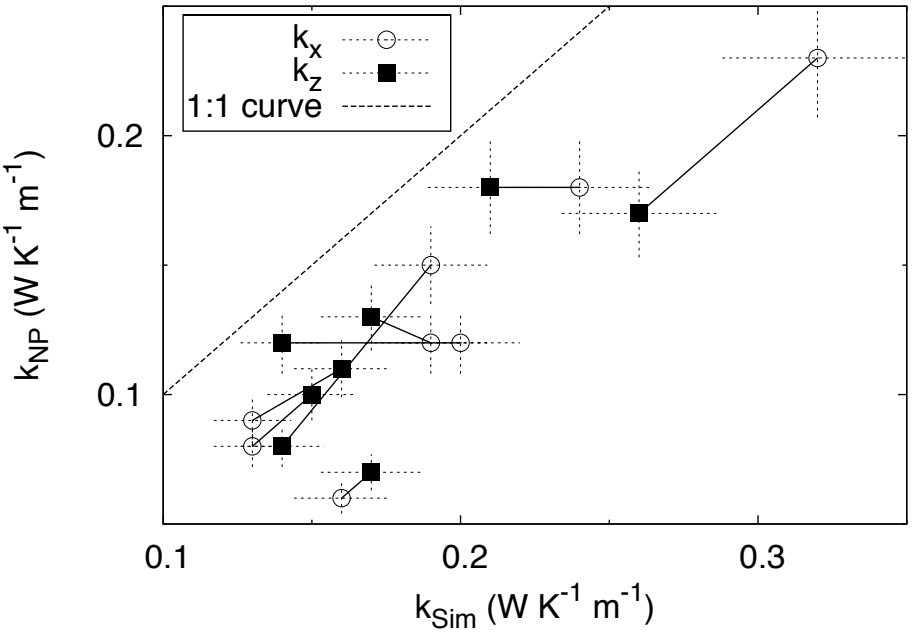

Fig. 3. Comparison of the horizontal and vertical component of the thermal conductivity from direct numerical simulation, k^{SIM} and needle probe, k^{NP}. All measurements except two show the same trend in anisotropy, however all components of $k^{NP}_{x,z}$ are systematically lower than $k^{SIM}_{x,z}$.

TCD
6, 1839–1869, 2012

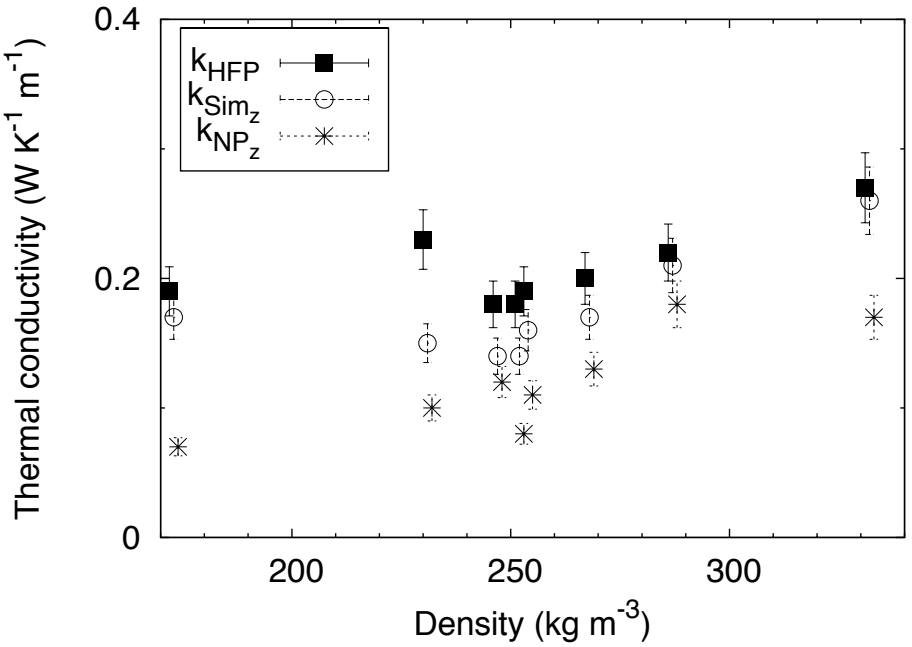

Fig. 4. Comparison of the vertical components of the thermal conductivity, k_z for all methods. HFP gave always the highest value and the needle probe the lowest one, the direct numerical simulation is close to HFP. The bars indicate the estimate of the measurement error.

TCD
6, 1839–1869, 2012

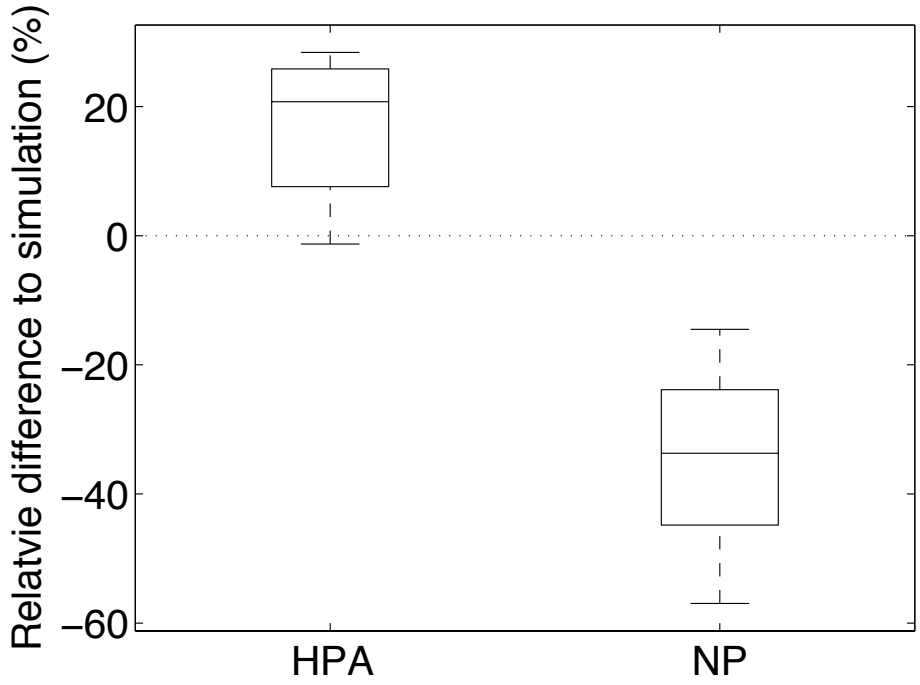

Fig. 5. Relative differences of k_z for the 8 samples used between HFP and NP with direct numerical simulation as reference. HFP measures 20 % too high, NP 35 % too low compared to the simulation. The median of the relative differences is the line inside the box; the top and the bottom of the boxes are the quartiles.

TCD
6, 1839–1869, 2012

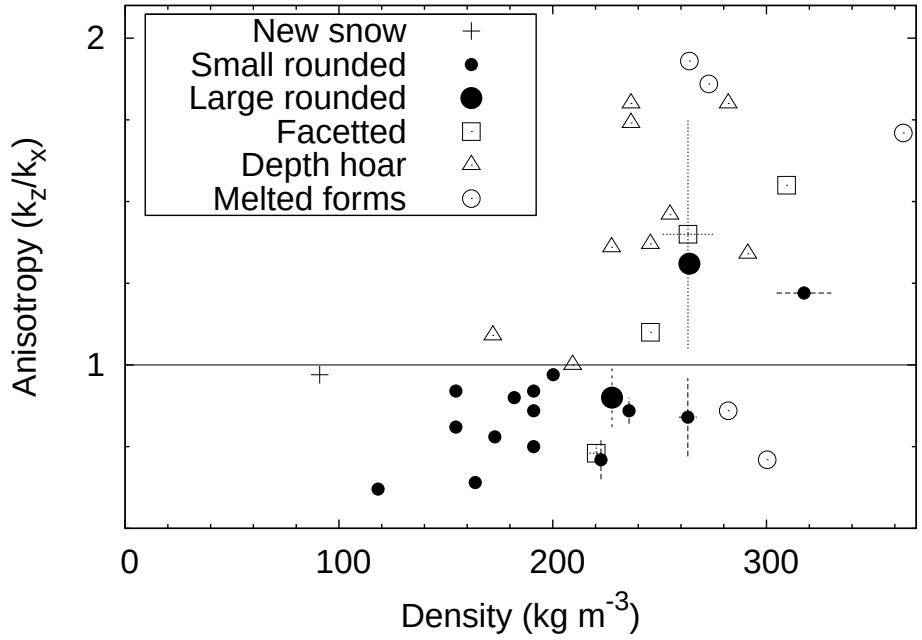

Fig. 6. Anisotropy factor α of different snow types as a function of density. The anisotropy used here was calculated by direct numerical simulation. The 8 samples measured with SIM, HPA and NP are indicated by large symbols and error bars. Other samples are indicated by small symbols.

TCD
6, 1839–1869, 2012